Experimental signatures of a nonequilibrium phase transition governing the yielding of a soft glass

K. Hima Nagamanasa,[1,*,†] Shreyas Gokhale,[2,*] A. K. Sood,[2,3] and Rajesh Ganapathy[3,†]

[1]*Chemistry and Physics of Materials Unit, Jawaharlal Nehru Centre for Advanced Scientific Research, Jakkur, Bangalore 560064, India*

[2]*Department of Physics, Indian Institute of Science, Bangalore 560012, India*

[3]*International Centre for Materials Science, Jawaharlal Nehru Centre for Advanced Scientific Research, Jakkur, Bangalore 560064, India*

(Received 4 December 2013; revised manuscript received 11 February 2014; published 17 June 2014; corrected 16 October 2014)

We present direct experimental signatures of a nonequilibrium phase transition associated with the yield point of a prototypical soft solid—a binary colloidal glass. By simultaneously quantifying single-particle dynamics and bulk mechanical response, we identified the threshold for the onset of irreversibility with the yield strain. We extracted the relaxation time from the transient behavior of the loss modulus and found that it diverges in the vicinity of the yield strain. This critical slowing down is accompanied by a growing correlation length associated with the size of regions of high Debye-Waller factor, which are precursors to yield events in glasses. Our results affirm that the paradigm of nonequilibrium critical phenomena is instrumental in achieving a holistic understanding of yielding in soft solids.

DOI: 10.1103/PhysRevE.89.062308 PACS number(s): 83.10.Tv, 82.70.Dd, 83.60.La, 83.80.Ab

I. INTRODUCTION

A wide variety of solids, including atomic crystals, metallic glasses, dense suspensions, gels and foams, exhibit yielding and plastic flow when subjected to sufficiently large external stresses [1,2]. Apart from representing an interesting class of nonequilibrium processes, these phenomena are routinely exploited in numerous industrial applications [3]. Elucidating mechanisms that govern yielding and plasticity therefore assumes fundamental as well as technological significance. In hard crystalline materials, yielding proceeds via the motion of well-defined topological defects called dislocations. While no such topological defects have been identified in amorphous solids, flipping of shear transformation zones is thought to be responsible for plastic deformation. In both crystalline as well as amorphous solids, however, it is now well established that microscopic irreversible yield events during plastic deformation occur collectively as intermittent avalanches with power-law size distribution [4–6]. Further, the observation of self-organized criticality in these systems suggests an underlying nonequilibrium phase transition [7,8], which theories and simulations posit to be centered at the yield point [9]. Together, these observations indicate the emergence of robust dynamical features near yielding that are insensitive to microscopic details.

By contrast, for soft solids, which encompass a broad class of materials including dense colloidal suspensions, gels and foams, a holistic understanding of yielding is yet to emerge. Thus far, a majority of the rheological studies on soft solids have been aimed at characterizing the bulk flow behavior and examining its dependence on the nature of the interparticle interactions [10–12] as well as the system's proximity to the jamming transition [13,14]. From the point of view of understanding the microscopic mechanisms that lead to yielding, however, relatively little is known. On this front, experiments on 2D colloidal crystals [15] have shown that local yield events, namely dislocations, move collectively and self-organize into avalanches that follow a power-law scaling identical to the one observed in atomic crystals. The collective nature of local plastic events has also been observed in sheared hard sphere colloidal glasses [16]. Further, recent indentation experiments [17,18] have shown that even in hard sphere glasses, correlations between local yield events result in avalanches whose size distribution follows a power-law scaling at the onset of rigidity, which led the authors to suggest that yielding could be associated with a critical phenomenon. However, since all the aforementioned studies employed steady shear, where the continuous accumulation of strain precludes the characterization of steady states [19,20], they were unable to establish even the existence of a critical phenomenon underlying yielding, let alone elucidate its nature. On the other hand, despite the fact that oscillatory shear allows steady states to be probed at all applied strains, it has received relatively less attention. One of the first advances in this direction was made by Hebraud *et al.* [21], who performed diffusive wave spectroscopy on periodically sheared concentrated emulsions and showed the existence of a finite threshold for the onset of irreversibility. By employing the same technique, Petekidis and coworkers [22] later showed that a similar threshold exists for hard sphere colloidal glasses as well. In addition, they showed that the growth of irreversibility with strain beyond its onset is governed by the volume fraction of the sample. Despite their utility in quantifying irreversibility, light-scattering techniques are not well suited either to probe the collective nature of local plastic events or to characterize the approach to steady state. These difficulties have been surmounted by optical microscopy-based studies, which facilitate not only the identification of irreversible events but also the investigation of their spatiotemporal evolution down to the single-particle level. Recent optical microscopy studies on two-dimensional (2D) jammed colloidal suspensions [23] have shown that irreversibility, characterized by the number of T1 events that lead to permanent changes in particle configurations, decreases with time on approaching steady state. Further, it was speculated that the steady-state number of these irreversible T1 events should increase sharply across the transition from reversible to irreversible dynamics near the yield point. Recent simulations on soft spheres [24]

*K.H.N. and S.G. contributed equally to this work.

†Corresponding authors.

appear to support this scenario. In Ref. [24], the authors characterized the onset of yielding at the particle scale from the mean-square displacement, a quantity proportional to the number of irreversible events, and correlated it with rheology at the macroscopic scale. They observed that the mean-squared displacement changes continuously on approaching the steady state for an applied strain and the diffusion coefficient, a measure of steady-state irreversibility, changes rapidly across the threshold strain. It was also speculated that the onset of irreversibility may be associated with an absorbing phase transition of the type observed in Ref. [25], although no evidence was presented. Despite these advances, important issues remain unresolved. In all the experiments discussed above, the yield strain has been estimated from independent rheological measurements and it is therefore unclear whether the microscopic threshold for irreversibility corresponds to the bulk yield point. Moreover, quantitative measurements of the relaxation time associated with the evolution of irreversibility on approaching steady state are still lacking. As a consequence, whether the observed correlations between local plastic events lead to a nonequilibrium phase transition at the yield point still remains an open question.

In this work, by combining particle scale imaging with bulk rheology we show that the transition from reversible to irreversible dynamics during yielding of a prototypical soft solid—a binary colloidal glass—shows signatures of a nonequilibrium critical phenomenon. By applying oscillatory shear of a wide range of amplitudes, we identified the threshold for the onset of irreversibility. We also extracted critical exponents for the order parameter and the relaxation time. A similar relaxation time exponent was observed in a very recent theoretical study based on nonequilibrium thermodynamics of shear transformation zones (STZs) in amorphous solids [26]. Further, the exponents observed in our experiments have also been seen in periodically driven dilute non-Brownian suspensions [25]. However, our results differ significantly from those in Ref. [25]. The most important distinction is that our particles are Brownian and, due to thermal fluctuations, the critical strain for the onset of irreversibility is identically zero in the dilute limit. It is only in sufficiently dense Brownian suspensions, where particle caging by neighbours results in finite rigidity, that the transition to irreversibility occurs at a nonzero strain [22]. Together, these features of Brownian suspensions enabled us to directly link the critical-like behavior of irreversible rearrangements with yielding of the glass. Further, while soft solids may not always share the phenomenology of hard systems [27], the striking similarities in the yielding of colloidal and atomic crystals [5,15] and glasses [16,28] suggest that insights gleaned from the present studies may be relevant to hard materials as well.

II. EXPERIMENTAL METHODS

Our system comprised of an aqueous suspension of temperature-sensitive size-tunable poly N-isopropylacryl amide (PNIPAM) colloidal spheres of radii of 1 and 2 μm. These particles were synthesized using a standard emulsion polymerization protocol [29] and were tagged with fluorophore rhodamine 6G to enable confocal imaging. The lower critical solution temperature for these particles is $\approx$38°C and

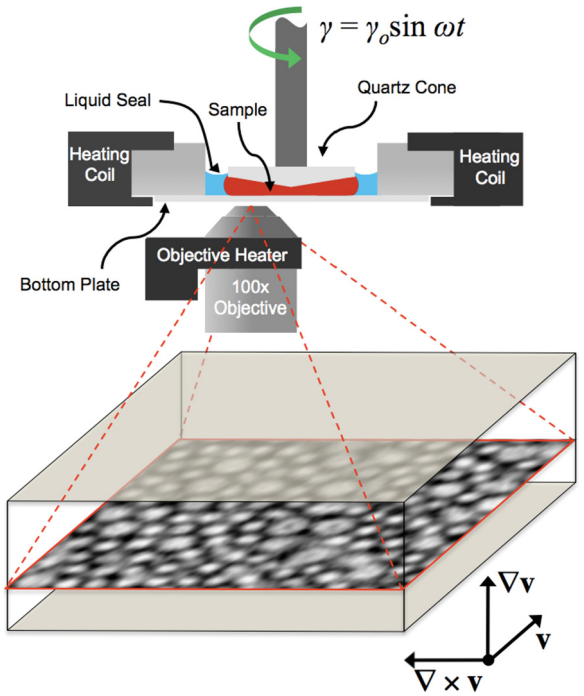

FIG. 1. (Color online) Schematic of the confocal rheometer.

the experiments were performed at $\approx$24°C. A number density ratio of 1:3 of large and small particles adequately suppressed crystallization, as confirmed by 3D confocal imaging. In addition, by counting the number of big and small particles in a given 3D confocal volume, we estimated the volume fraction of our system to be $\phi \approx 0.67$. By combining a fast confocal microscope with a rheometer (Fig. 1) [30], we investigated the particle scale dynamics of the glass under shear. Our apparatus consisted of a commercial stress-controlled rheometer (MCR-301, Anton Paar), mounted on a fast confocal microscope (Visitech VT-Eye confocal scanner coupled to Leica DMI 6000B microscope) using a home-made mechanical stage. Imaging was performed using a 100×, N.A. 1.4, oil immersion Plan Apochromat Leica objective. The experiments were carried out in a home-made shear cell using a cone-plate geometry. A quartz cone of diameter 25 mm and cone angle 1° and a cover glass of thickness 170 μm were used as the top and the bottom plates, respectively. An immobilized layer of particles on the top and the bottom plates prevented wall slip. After loading, the samples were subjected to a temperature quench to ensure homogenization. In addition, to maintain identical initial conditions for all measurements, the samples were presheared at a constant strain rate of 5 s^{-1} for 3 min, following which a waiting time of 5 min was observed prior to every measurement. Following preshear, the bulk elastic and viscous moduli G' and G'', respectively, were measured by applying oscillatory strains $\gamma = \gamma_o \sin \omega t$, where γ_o is the strain amplitude and ω is the frequency. Subsequently, we measured G' and G'' as a function of the oscillation cycle number τ for various γ_o's at $\omega = 1$ rad/s. For each γ_o, single-particle dynamics were quantified by imaging a 54 × 54 μm 2D slice oriented parallel to the velocity-vorticity plane and located 7 μm away from the fixed bottom plate, at 60 frames per second. To visualize the 3D microstructure, we

obtained image stacks ($25 \times 25 \times 8$ μm) along the velocity gradient direction at a few select γ_o's. The single-particle dynamics were quantified using standard particle tracking algorithms [31] as well as codes developed in-house.

III. RESULTS AND DISCUSSION

The rheological response of our sample is typical of a soft glass [Fig. 2(a)] [10–12]. We found only a weak dependence of G' and G'' on ω, which independently confirmed that our samples were in the glassy state (inset to Fig. 2) [10]. From γ_o-sweep experiments, it is evident that for the volume fraction used here, the system is a viscoelastic solid in the zero strain limit. The plateau modulus G' observed here is low as compared to what is typically seen for microgels, suggesting that the major contribution to elasticity comes from particle caging and jamming [12] rather than the interpenetration of the polymer chains themselves. With increasing γ_o we find that the system goes from a viscoelastic solid to a viscoelastic liquid with a well-defined G'-G'' crossover, which is a crucial requirement from the point of view of identifying the threshold for irreversibility with the yield strain. The γ_o corresponding to the crossover of G' and G'' was identified as the yield strain $\gamma_y = 0.2$ [12]. The ubiquitous G'' peak was located beyond γ_y [Fig. 2(a)]. The Péclet number of our system, defined as $\mathrm{Pe} = \omega\tau_B$ [32], is 1.92. Here $\omega = 1$ rad/s is the frequency of applied strain and $\tau_B = R^2/D_o = 6\pi\eta R^3/k_BT$ is the Brownian time of the particles. Pe was estimated by taking R to be the mean radius of our particles (0.75 μm) and using the solvent viscosity $\eta = 0.001$ Pa s. The high Pe combined with the position of the G'' peak suggests that yielding in our system may be governed by shear-induced rearrangements rather than thermally assisted cage jumps [32]. Moreover, from an independent set of experiments, we observed that in concord with [32], the G'' peak shifts further away from the crossover with increasing ω [Fig. 2(b)]. This suggests that the location of the G'' is correlated with the relative importance of thermally activated and shear-induced rearrangements.

Next we characterized the irreversible microstructural changes that lead to yielding. A natural measure of irreversibility is the fraction, f_{IR}, of particles that do not return to their initial positions at the end of a strain cycle [25]. Since f_{IR} is independent of the exact nature of local yield events, it should be generically applicable to ordered as well as disordered soft solids. We first identified the irreversible events (IRs) in 3D. Here, the time resolution between two successive confocal z stacks was too small to allow the construction of individual particle trajectories. We therefore used a protocol based on pattern matching to estimate macroscopic drift and to identify IRs. As the strain threshold for displacement of large particles is greater than that of the small ones, we used only large particles to estimate the drift. The drift was calculated by displacing one z stack with respect to the other in both X and Y directions and finding the displacements X_d and Y_d, for which the overlap between the two stacks is maximum. We then used the drift-corrected particle positions to identify IRs. A particle was labeled irreversible if, at the end of the strain cycle, it did not return to its initial position within a distance of $\sigma/2$, where σ is the particle diameter. Confocal volumes highlighting irreversible events show that f_{IR} exhibits an increase across γ_y [33] (Fig. 3). Further, f_{IR} predominantly comprises small particles due to their lower strain threshold for irreversible rearrangements. However, as the displacement of large particles also becomes significant with increasing γ_o, this procedure is reliable only at small and moderate γ_o's.

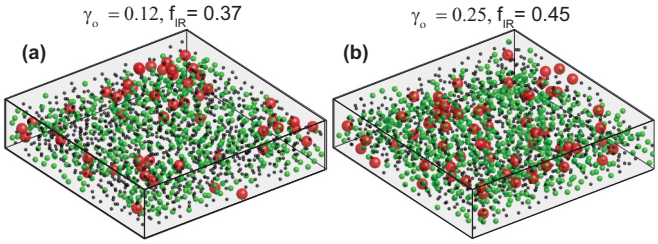

FIG. 3. (Color online) [(a) and (b)] Reconstruction of 3D volumes of the sample for $\gamma_o = 0.12$ and 0.25, respectively. Large and small irreversible particles are rendered as red and green spheres, respectively, and the reversible ones are shown as black spheres.

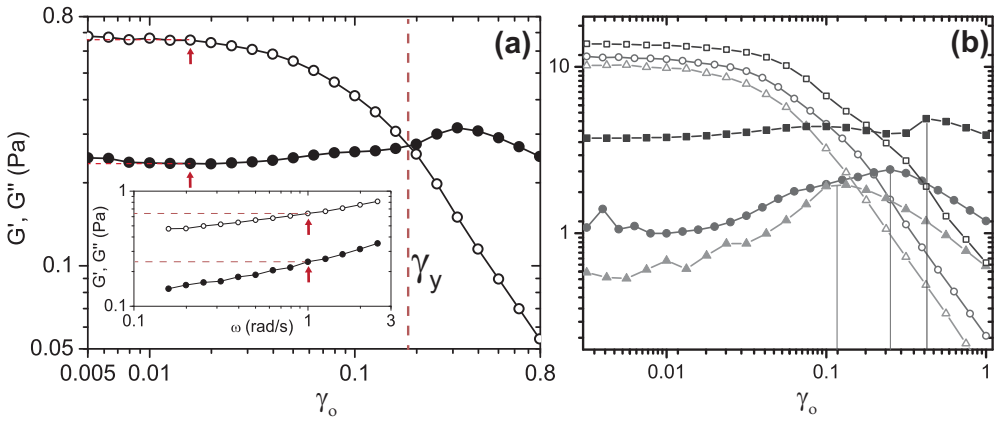

FIG. 2. (Color online) (a) γ_o-sweep measurements performed at $\omega = 1$ rad/s. Inset shows results from ω-sweep experiments at $\gamma_o = 0.015$. G' and G'' are denoted by (○) and (●), respectively. The red arrows and dotted lines in the figure and the inset highlight the values of G' and G'' for $\gamma_o = 0.015$ and $\omega = 1$ rad/s. (b) γ_o - sweep experiments for $\omega = 0.1$ rad/s (▲), $\omega = 1$ rad/s (●) and $\omega = 20$ rad/s (■). G' and G'' are denoted by open and filled symbols respectively. The solid lines highlight the γ_o corresponding to the G'' peak.

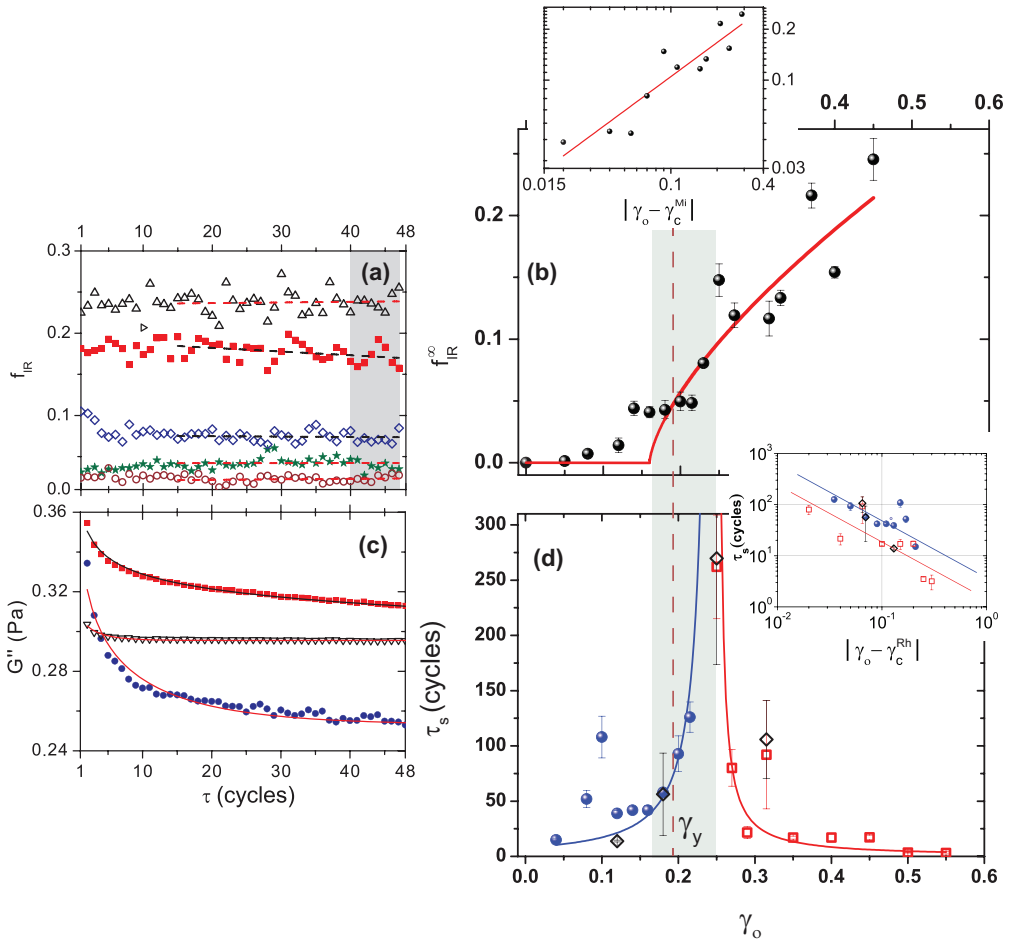

FIG. 4. (Color online) (a) $f_{IR}(\tau)$ for $\gamma_o = 0.05$ (○), $\gamma_o = 0.12$ (★), $\gamma_o = 0.215$ (◇), $\gamma_o = 0.25$ (■), and $\gamma_o = 0.37$ (△). The dashed lines are linear fits to the data. (b) f_{IR}^{∞} as a function of γ_o. Inset to (b) shows f_{IR}^{∞} versus $|\gamma_o - \gamma_c^{Mi}|$. $f_{IR}^{\infty}(\gamma_o) = f_{IR}^{ss}(\gamma_o) - f_{IR}(\gamma_o = 0)$, where f_{IR}^{ss} is the steady-state fraction of irreversible rearrangements obtained by averaging over the shaded region in A. The thermal contribution to f_{IR}, $f_{IR}(\gamma_o = 0) = 0.023$. The red curve is a power-law fit to the data. γ_c^{Mi} and β were extracted by minimizing χ^2. (c) $G''(\tau)$ for $\gamma_o = 0.04$ (●), $\gamma_o = 0.25$ (■), and $\gamma_o = 0.45$ (▽). The curves are best fits to the data. A power-law exponent $\delta = 0.27 \pm 0.02$ was found to give satisfactory fits for all γ_o's. (d) Relaxation time τ_s versus γ_o. The solid curves represent power laws of the form $|\gamma_o - \gamma_c^{Rh}|^{-1.5}$ (blue) and $|\gamma_o - \gamma_c^{Rh}|^{-1.1}$ (red) and serve as guides to the eye. The inset to (d) shows τ_s versus $|\gamma_o - \gamma_c^{Rh}|$. Since $\gamma_o = 0.25$ corresponds to the critical strain γ_c^{Rh}, it cannot be represented on a double logarithmic plot and is therefore not shown in the inset. The red line is a fit to the data for $\gamma_o > \gamma_c^{Rh}$ (□). For $\gamma_o < \gamma_c^{Rh}$ (●), the presence of outliers precludes satisfactory linear fitting and, hence, the blue line shown is a guide to the eye with the same slope as the red line. Black diamonds (◇) correspond to τ_s obtained from independent measurements on the same sample. The fitting uncertainties in (b) and (d) are standard errors.

Due to the poor temporal resolution in 3D imaging at large γ_o's, we resorted to 2D to quantify $f_{IR}(\tau)$ for all γ_o's investigated. The high frame rate used to capture 2D slices is sufficient to track individual particles and hence standard procedures were used to obtain particle displacements [31]. Here, to set the displacement threshold for IRs, we plotted the distribution of displacements in the first cycle for each γ_o. The value of displacement beyond which the distributions exhibited deviations from Gaussian behavior was chosen as the threshold for identifying IRs. Also, as shear induces anisotropy in displacements, the threshold was chosen independently for the X and Y directions. We find that for $\gamma_o < \gamma_y$, the thresholds in the X and Y directions are $0.31 \pm 0.08\sigma$ and $0.32 \pm 0.08\sigma$ respectively, whereas for $\gamma_o > \gamma_y$, they are $0.39 \pm 0.1\sigma$ and $0.44 \pm 0.1\sigma$. Here σ is the mean diameter of the big and the small particles. Further, we also checked the nearest-neighbor configurations for all the particles that underwent large displacements. Particles separated by a distance less than 1.4σ, which corresponds to the first minimum of the radial pair correlation function, were identified as nearest neighbors. Since we only tracked particles in the XY plane, we lack information about displacements in the Z direction. However, it is likely that if a trajectory is terminated due to out-of-plane motion, then the particle made a large displacement. Hence, all such particles were also identified as lost neighbors. A particle was then labeled irreversible if it made a displacement greater than the threshold and lost at least four neighbors at the end of the strain cycle. Studies on supercooled liquids and glasses have shown that configurational changes ensuing from such irreversible dynamics are permanent [34,35]. For γ_o's far from γ_y, we did not observe any transients in $f_{IR}(\tau)$, implying that steady state was reached rapidly [Fig. 4(a)].

Near γ_y, for $\gamma_o = 0.25$, however, $f_{\rm IR}(\tau)$ shows a slow fall over the experimental duration. Similar long-lived transients near yielding have also been observed in recent simulations of periodically sheared amorphous solids [36]. To investigate the onset and γ_o dependence of irreversibility, we plotted the steady-state fraction of irreversible particles after subtracting the thermal contribution, denoted by $f_{\rm IR}^{\infty}$, as a function of γ_o in Fig. 4(b) (Supplemental Material Movie S1 [37]). $f_{\rm IR}^{\infty}$ shows a modest rise up to a critical strain $\gamma_c^{\rm Mi}$ and increases more rapidly beyond $\gamma_c^{\rm Mi}$ [22]. Here, the superscript "Mi" signifies that the critical strain has been extracted from microscopy data. It is quite conceivable that $f_{\rm IR}^{\infty}$ behaves as an order parameter for irreversibility. By fitting $f_{\rm IR}^{\infty}$ with a power law of the form $f_{\rm IR}^{\infty} \propto (\gamma_o - \gamma_c^{\rm Mi})^{\beta}$ for $\gamma_o > \gamma_c^{\rm Mi}$, we extracted an 'order parameter exponent' $\beta = 0.67 \pm 0.09$ and a "critical strain" $\gamma_c^{\rm Mi}$ of 0.16, which is close to γ_y [inset to Fig. 4(b)].

The dependence of $f_{\rm IR}^{\infty}$ on γ_o suggests a nonequilibrium phase transition governing yielding and it is therefore natural to wonder whether the long-lived transients in $f_{\rm IR}(\tau)$ correspond to critical slowing down. Since irreversible dynamics leads to energy dissipation, the transients in $f_{\rm IR}$ are also evident in $G''(\tau)$ [Fig. 4(c)]. Unlike $f_{\rm IR}(\tau)$, $G''(\tau)$ is a bulk measure and therefore has a significantly better signal-to-noise ratio. Analogously to Ref. [25], the relaxation curves in Fig. 4(c) are well fitted by the functional form $G''(\tau) = (G_o'' - G_{\infty}'')\frac{e^{-\tau/\tau_s}}{\tau^{\delta}} + G_{\infty}''$, where τ_s is the time taken to reach steady state and G_o'' and G_{∞}'' are the initial- and steady-state values of $G''(\tau)$, respectively. This functional form captures the crossover from exponential to power-law behavior expected near a critical point. Remarkably, τ_s extracted from the fits appears to diverge at a critical strain $\gamma_c^{\rm Rh} = 0.25$ close to γ_y [Fig. 4(d)]. Here, the superscript "Rh" denotes that the critical strain has been extracted from rheology data. By fitting τ_s with a power law of the form $\tau_s \propto |\gamma_o - \gamma_c^{\rm Rh}|^{-\alpha}$ for $\gamma_o > \gamma_c$, we obtained the relaxation time exponent $\alpha = 1.1 \pm 0.3$ [inset to Fig. 4(d)]. Although the dynamical range covered here is insufficient to extract reliable exponents, it is encouraging that the same relaxation time exponent was predicted in a recent theoretical study on periodically sheared amorphous solids [26]. Collectively, from our observations [Figs. 4(b) and 4(d)] it is tempting to speculate that yielding of colloidal glasses is associated with a nonequilibrium critical point.

Yielding in hard materials has often been associated with the pinning-depinning transition [9]. However, quenched disorder, which is an important ingredient of pinning-depinning transitions, is absent in our system. The γ_o dependence of $f_{\rm IR}^{\infty}$ observed here suggests a transition from reversible dynamics with $f_{\rm IR}^{\infty} \approx 0$ to irreversible dynamics with $f_{\rm IR}^{\infty} > 0$, which is characteristic of an absorbing phase transition (APT) [25]. Most APTs belong to the directed percolation universality class [38]. However, the particle number density being conserved in our system, the putative nonequilibrium phase transition associated with yielding may belong to the conserved directed percolation (C-DP) universality class [39]. Further, in our cone-plate shear geometry, the diameter of the cone is ~200 times larger than the gap and, hence, the critical exponents extracted here should therefore be in agreement with those observed for 2D C-DP [39]. Interestingly, we find that the relaxation time exponent $\alpha = 1.1 \pm 0.3$ [Fig. 4(d)] and the order parameter exponent $\beta = 0.67 \pm 0.09$ [Fig. 4(b)] are indeed very close to the C-DP universality class value in 2D [39]. However, within experimental uncertainty, it is not possible to ascertain the universality class of the yielding transition.

The observation of critical slowing down implies increasing spatial correlations between local irreversible rearrangements near yielding. In our system, these correlations can be probed using concepts developed to understand the dynamics of amorphous solids. Recent simulations suggest that local plastic events in glasses originate from spatially localized low-frequency vibrational modes [40]. Since these localised regions also posses low stiffness values, we identified them using a local measure of elasticity, namely the Debye-Waller factor u_i [41] defined as $u_i = (r_i - \langle r_i \rangle)^2$ [42]. Here r_i is the instantaneous position of particle i, and $\langle r_i \rangle$ is its mean position averaged over a suitable time window. To choose this window, we adopted a procedure analogous to the one routinely used for quantifying dynamical heterogeneities in supercooled liquids [43]. Accordingly, for each γ_o, for different time windows Δt, with Δt being less than the cage-breaking time, we clustered the top 10% of the high-u_i particles based on nearest-neighbor distances. We find that the average cluster size as a function of time exhibits a maximum at $\Delta t = t_{\rm max}$, which was chosen to be the appropriate time interval for computing u_i. Experimentally, u_i is a fairly accurate measure since it requires particles to be tracked only for a short duration. Figure 5(a) shows a color map of u_i averaged over an oscillation cycle for $\gamma_o = 0.25$ and $\tau = 2$ and the inset shows its distribution $P(u_i)$. We find that regions of high u_i are spatially localized and correlated with subsequent irreversible rearrangements [gray circles in Fig. 5(a)]. The transient dynamics of $f_{\rm IR}(\tau)$ [Fig. 4(a)] should therefore stem from the spatiotemporal evolution of these high-u_i regions. To show this, we first identified the top 10% of the high-u_i particles for various γ_o's. Figures 5(b) and 5(c) show snapshots of these particles for $\gamma_o = 0.27$ at $\tau = 2$ and 47, respectively. The top 10% of the high-u_i particles are spatially clustered and, more importantly, there are fewer large clusters for $\tau = 47$. Figures 5(d)–5(f) shows the cluster size distribution $P(n)$, where n is the number of particles in a cluster, for three different time intervals at various γ_o's. Analogously to $f_{\rm IR}(\tau)$, $P(n)$ is stationary for γ_o far from $\gamma_c^{\rm Rh}$ and evolves steadily in the vicinity of $\gamma_c^{\rm Rh}$. Further, near $\gamma_c^{\rm Rh}$, $P(n)$ for $n > 20$ is significantly smaller at a larger τ. It is also evident that, on average, clusters are larger for $\gamma_o \approx \gamma_c^{\rm Rh}$ [Fig. 5(e)] as compared to γ_o far away from $\gamma_c^{\rm Rh}$ [Figs. 5(d) and 5(f)]. Indeed, the average cluster size $\langle n \rangle = \frac{\sum n^2 P(n)}{\sum n P(n)}$, a commonly used measure of the correlation length [44], shows a clear maximum near $\gamma_c^{\rm Rh}$ [Fig. 5(g)].

Our results strongly suggest that correlations between local yield events not captured by mean-field theories like soft glassy rheology (SGR) [45] lead to a nonequilibrium phase transition at the yield point. For γ_o less than a critical strain, yield events are rare and the system appears to self-organize quickly into an "absorbing" steady state ($f_{\rm IR}^{\infty} \approx 0$), where the applied strain is insufficient to induce irreversible changes in particle configuration. For γ_o larger than the critical strain, the imposed strain facilitates many independent irreversible

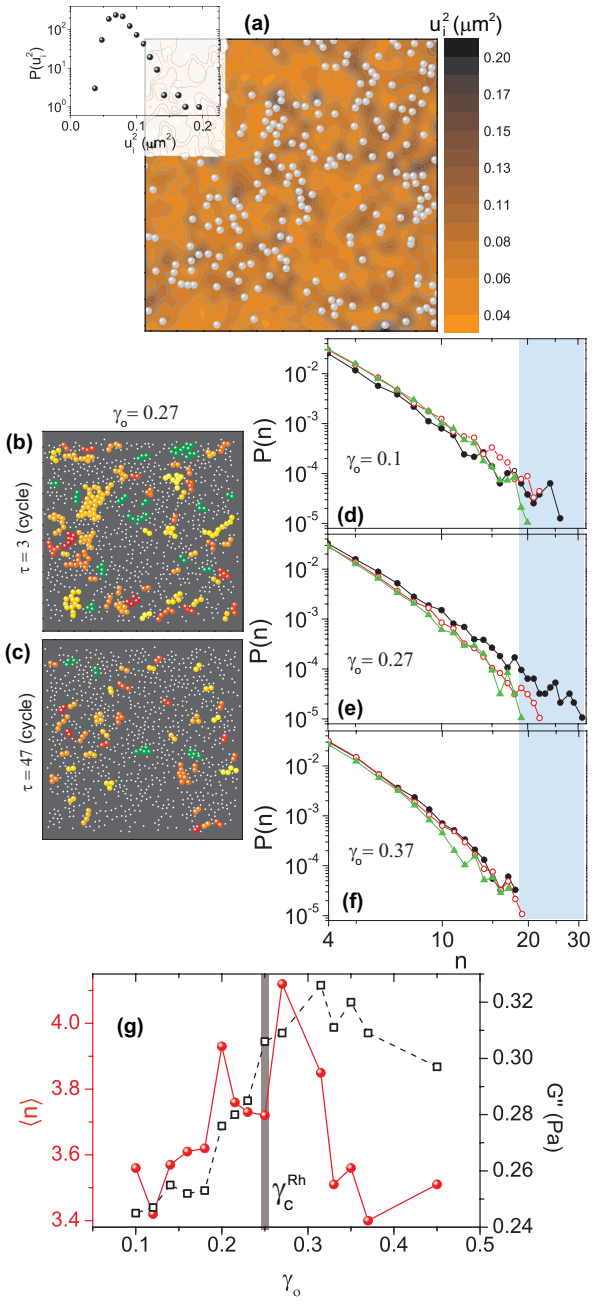

FIG. 5. (Color online) (a) Color map of u_i for $\tau = 2$. The solid spheres represent irreversible particles at the end of the same cycle. Inset shows the distribution of u_i. [(b) and (c)] Representative snapshots with the top 10% of the high-u_i particles shown as big solid spheres and the remaining shown as small circles. The colors are a visual aid to help demarcate clusters. [(d)–(f)] Distribution of cluster size $P(n)$. In (d)–(f) $P(n)$ for $\tau = 2$ to 10 (●), for $\tau = 20$ to 30 (○), and for $\tau = 37$ to 47 (▲). (g) $\langle n \rangle$ as a function of γ_o is shown as (●). G'' from bulk rheology is shown as (□).

rearrangements, correlations between yield events are washed out, and the system rapidly reaches a "fluctuating" steady state ($f_{IR}^{\infty} > 0$) [45]. Close to the critical strain, however, correlations between local yield events trigger a cascade of irreversible rearrangements, which is manifested as a growing length scale [Fig. 5(g)] and leads to critical slowing down [Fig. 5(d)]. Further, it has not skipped our attention that the growing cluster sizes near γ_y may also have implications for the origin of the G'' peak [Fig. 5(g)]. This is especially important when the G'' peak coincides with the yield strain, a scenario frequently observed in soft solids.

IV. CONCLUSION

To summarize, through simultaneous quantification of single-particle dynamics and bulk viscoelastic moduli, we have uncovered signatures of a nonequilibrium critical phenomenon governing yielding of a colloidal glass [Figs. 4(b) and 4(d)]. Unlike non-Brownian suspensions, our Brownian system has a finite threshold for irreversibility only at sufficiently large volume fractions where it behaves as a viscoelastic solid. This enabled us to identify the observed critical point with the yield strain. The excellent agreement between the experimental [Fig. 4(d)] and theoretical [26] values of the exponent characterizing the divergence in the relaxation time is worthy of further investigation. We found that the growing time scale in our experiments is accompanied by a growing length scale associated with clusters of particles with a high Debye-Waller factor [Fig. 5(g)], which are precursors of local plastic events in amorphous solids [Fig. 5(a)]. We therefore expect the correlations between local irreversible rearrangements observed here to have a correspondence with observations of avalanches in sheared amorphous solids [28]. In the context of soft colloidal systems like star polymers and microgels, it would be interesting to study the influence of particle softness on the nature of the yielding transition. More generally, given that a wide range of soft materials such as gels, emulsions, and foams also exhibit strikingly similar rheological properties, the transition observed here should be generic to soft solids and similar studies on diverse soft systems are required to verify this claim. Although the mechanical response of soft solids depends only weakly on frequency, it would be worthwhile to examine the frequency dependence of the onset of irreversibility in these materials. Our results exemplify the need for refining mean field theories like SGR. In particular, it might be possible to incorporate explicit interactions in SGR such that the local yielding of one element assists in the yielding of a neighboring element. Connections of such an extended SGR model to theories that relate yielding to the percolation of a liquid phase within a deformed solid [46] may also be conceivable. Most importantly, our findings set the stage for developing a unified framework for yielding of soft solids.

ACKNOWLEDGMENTS

The authors thank Michael Cates, Jack Douglas, Sriram Ramaswamy, Narayanan Menon, and Rema Krishnaswamy for helpful discussions. K.H.N. thanks the Council for Scientific and Industrial Research (CSIR) India for a Senior Research Fellowship. S.G. thanks CSIR India for a Shyama Prasad Mukherjee Fellowship. A.K.S. thanks Department of Science and Technology, India, for support under a J.C. Bose Fellowship and R.G. thanks the International Centre for Materials Science (ICMS) and the Jawaharlal Nehru Centre for Advanced Scientific Research (JNCASR) for financial support.

[1] C. Miguel and M. Rubi, *Jamming, Yielding, and Irreversible Deformation in Condensed Matter* (Springer-Verlag, Berlin, 2006).

[2] H. A. Barnes, J. Non-Newtonian Fluid Mech. **81**, 133 (1999).

[3] R. Valiev, Nat. Mater. **3**, 511 (2004).

[4] D. M. Dimiduk, C. Woodward, R. LeSar, and M. D. Uchic, Science **312**, 1188 (2006).

[5] M.-C. Miguel, A. Vespignani, S. Zapperi, J. Weiss, and J.-R. Grasso, Nature **410**, 667 (2001).

[6] B. A. Sun, H. B. Yu, W. Jiao, H. Y. Bai, D. Q. Zhao, and W. H. Wang, Phys. Rev. Lett. **105**, 035501 (2010).

[7] P. Bak, C. Tang, and K. Wiesenfeld, Phys. Rev. Lett. **59**, 381 (1987).

[8] P. Bak, C. Tang, and K. Wiesenfeld, Phys. Rev. A **38**, 364 (1988).

[9] G. Tsekenis, J. Uhl, N. Goldenfeld, and K. Dahmen, Europhys. Lett. **101**, 36003 (2013).

[10] P. Sollich, Phys. Rev. E **58**, 738 (1998).

[11] V. Carrier and G. Petekidis, J. Rheol. **53**, 245 (2009); B. M. Erwin, M. Cloitre, M. Gauthier, and D. Vlassopoulos, Soft Matter **6**, 2825 (2010); S. A. Rogers, B. M. Erwin, D. Vlassopoulos, and M. Cloitre, J. Rheol. **55**, 733 (2011); S. A. Rogers, B. M. Erwin, D. Vlassopoulos, and M. Cloitre, **55**, 435 (2011).

[12] K. van der Vaart, Y. Rahmani, R. Zargar, Z. Hu, D. Bonn, and P. Schall, J. Rheol. **57**, 1195 (2013).

[13] K. N. Nordstrom, E. Verneuil, P. E. Arratia, A. Basu, Z. Zhang, A. G. Yodh, J. P. Gollub, and D. J. Durian, Phys. Rev. Lett. **105**, 175701 (2010).

[14] A. Basu, Y. Xu, T. Still, P. E. Arratia, Z. Zhang, K. N. Nordstrom, J. M. Rieser, J. P. Gollub, D. J. Durian, and A. G. Yodh, Soft Matter **10**, 3027 (2014).

[15] A. Pertsinidis and X. S. Ling, New J. Phys. **7**, 33 (2005).

[16] V. Chikkadi, G. Wegdam, D. Bonn, B. Nienhuis, and P. Schall, Phys. Rev. Lett. **107**, 198303 (2011).

[17] Y. Rahmani, R. Koopman, D. Denisov, and P. Schall, Sci. Rep. **3**, 1064 (2013).

[18] Y. Rahmani, R. Koopman, D. Denisov, and P. Schall, Phys. Rev. E **89**, 012304 (2014).

[19] A. Fall, J. Paredes, and D. Bonn, Phys. Rev. Lett. **105**, 225502 (2010).

[20] T. Divoux, D. Tamarii, C. Barentin, and S. Manneville, Phys. Rev. Lett. **104**, 208301 (2010).

[21] P. Hébraud, F. Lequeux, J. P Munch, and D. J. Pine, Phys. Rev. Lett. **78**, 4657 (1997).

[22] G. Petekidis, A. Moussaïd, and P. N. Pusey, Phys. Rev. E **66**, 051402 (2002).

[23] N. C. Keim and P. E. Arratia, Soft Matter **9**, 6222 (2013).

[24] L. Mohan, C. Pellet, M. Cloitre, and R. Bonnecaze, J. Rheol. **57**, 1023 (2013).

[25] L. Corte, P. Chaikin, J. Gollub, and D. Pine, Nat. Phys. **4**, 420 (2008).

[26] N. Perchikov and E. Bouchbinder, Phys. Rev. E **89**, 062307 (2014).

[27] G. L. Hunter and E. R. Weeks, Rep. Prog. Phys. **75**, 066501 (2012).

[28] A. Lemaître and C. Caroli, Phys. Rev. Lett. **103**, 065501 (2009).

[29] D. B. Lawrence, T. Cai, Z. Hu, M. Marquez, and A. Dinsmore, Langmuir **23**, 395 (2007).

[30] S. Gokhale, K. H. Nagamanasa, V. Santhosh, A. Sood, and R. Ganapathy, Proc. Natl. Acad. Sci. USA **109**, 20314 (2012).

[31] J. C. Crocker and D. G. Grier, J. Colloid Interface Sci. **179**, 298 (1996).

[32] N. Koumakis, J. F. Brady, and G. Petekidis, Phys. Rev. Lett. **110**, 178301 (2013).

[33] M. Lundberg, K. Krishan, N. Xu, C. S. O'Hern, and M. Dennin, Phys. Rev. E **77**, 041505 (2008).

[34] A. Widmer-Cooper, H. Perry, P. Harrowell, and D. R. Reichman, Nat. Phys. **4**, 711 (2008).

[35] P. Yunker, Z. Zhang, K. B. Aptowicz, and A. G. Yodh, Phys. Rev. Lett. **103**, 115701 (2009).

[36] D. Fiocco, G. Foffi, and S. Sastry, Phys. Rev. E **88**, 020301 (2013); I. Regev, T. Lookman, and C. Reichhardt, *ibid.* **88**, 062401 (2013).

[37] See Supplemental Material at http://link.aps.org/supplemental/10.1103/PhysRevE.89.062308 for Movie S1. Movie S1 shows stroboscopic imaging of the binary colloidal glass under shear. The left and the right panels correspond to $g_o = 0.05$ and 0.25 respectively. The movie is played at a frame rate of 4 strain oscillation cycles per second.

[38] H. Hinrichsen, Adv. Phys. **49**, 815 (2000).

[39] G. I. Menon and S. Ramaswamy, Phys. Rev. E **79**, 061108 (2009).

[40] A. Tanguy, B. Mantisi, and M. Tsamados, Europhys. Lett. **90**, 16004 (2010).

[41] M. Tsamados, A. Tanguy, C. Goldenberg, and J.-L. Barrat, Phys. Rev. E **80**, 026112 (2009).

[42] A. Widmer-Cooper and P. Harrowell, Phys. Rev. Lett. **96**, 185701 (2006).

[43] F. W. Starr, J. F. Douglas, and S. Sastry, J. Chem. Phys. **138**, 12A541 (2013).

[44] E. R. Weeks, J. C. Crocker, A. C. Levitt, A. Schofield, and D. A. Weitz, Science **287**, 627 (2000).

[45] P. Sollich, F. Lequeux, P. Hébraud, and M. E. Cates, Phys. Rev. Lett. **78**, 2020 (1997).

[46] S. Liu, W. Jiao, B. Sun, and W. Wang, J. Non-Cryst. Solids **376**, 76 (2013).